Power Absorption in Ferromagnetic Implants from Radio Frequency Magnetic Fields and the Problem of Optimization

Shah A. Haider, *Student Member, IEEE*, Thomas C. Cetas *Member, IEEE*, James R. Wait, *Fellow, IEEE*, and Jong-S. Chen

Abstract—**Explicit expressions for absorbed power in small ferromagnetic cylinders from a radio frequency magnetic field (using a quasi-static approximation) due to induced eddy current circulation are obtained for implants used in interstitial hyperthermic therapy. It is found that optimum power absorption per unit volume of cylindrical implant occurs when the applied magnetic field is parallel to the axis of the cylinder and the induction number (i.e., $\sqrt{2}$ times the ratio of implant radius to skin depth) is 2.5. This result is used to design geometrical configurations for implants to achieve optimum heating effects. The dependence of absorbed power on the orientation of the cylindrical implant with respect to polarization of the magnetic field is also calculated and found to be in good agreement with experimental results.**

Introduction

THE ferromagnetic implants used in interstitial hyperthermia are usually needle shaped, and apart from end effects, can be represented by a cylindrical model. The power absorption in these implants from a time varying magnetic field is primarily due to resistive heating from the induced eddy currents circulating about the circumference of the implant. The heated implant in turn elevates the temperature of surrounding tissues by thermal conduction. We investigate here the nature of power absorption and its explicit dependence on implant material properties (electrical conductivity σ, and magnetic permeability μ), size (implant diameter), frequency and orientation of the implant with respect to field polarization to optimize the efficiency of heating.

The implant material is assumed to be homogeneous and isotropic. It is assumed also that electrical conductivity σ, magnetic permeability μ, dielectric constant ϵ, are real and do not depend on field strength and frequency within the range of application which are about $1000 \sim 2000$ A/m and $80 \sim 110$ kHz, respectively. Ferromagnetic materials developed for hyperthermia [1] in fact do exhibit some hysteresis loss although it has been found to be only a few percent of eddy current losses [2]. This justifies the assumption that μ is real by neglecting its relatively small imaginary part. Implant materials which might have significant hysteresis losses could be accommodated by introducing a complex permeability μ.

We consider here only the interaction of these ferromagnetic implants in a magnetic field. While the effects within an impressed electric field are interesting in other applications, the coils which generate the magnetic field are designed specifically to have very small associated axial and radial electric fields within the aperture occupied by a patient. That is, they are wound in a null sense with regard to the electric field or they have Faraday shields incorporated to suppress the electric field [11]. Finally, for perspective, the coils are large with diameters ranging from 0.3 to 0.7 m to accommodate patients while the implants (1 mm diameter, 20 to 100 mm long) and the implanted volume (10 to 1000 cm^3 with implant density approximately 1 cm of implant for each cm^3 of tumor) are small by comparison. Hence loading of the coil by the patient ($\mu = \mu_0$) and the implants is negligible, as is borne out in over 100 clinical treatments.

Power Absorption by a Cylindrical Implant in Axial Magnetic Field

A coil which is large enough to accommodate patients and which is excited by a radio frequency (say, 50 kHz to 500 kHz) current will generate reasonably uniform axial magnetic fields over volumes encompassing tumors of clinical relevance. Fields will vary radially within a ferromagnetic implant because of the finite conductivity σ and permeability μ. The time-harmonic uniform magnetic field polarized in the axial direction can be represented in cylindrical coordinates (ρ, ϕ, z) with the z-axis being coincident with implant axis. The z-directed magnetic field H_z will satisfy the scalar Helmholtz's equation [3]:

$$(\nabla^2 - \gamma^2) H_z = 0, \qquad \text{for } 0 \leqslant \rho \leqslant a \tag{1}$$

$$\gamma^2 = [\, j\omega\mu(\sigma + j\omega\epsilon)] \tag{2}$$

where γ is the propagation constant, ∇^2 is the cylindrical Laplacian operator, and a is the implant radius. Since the

Manuscript received August 27, 1990; revised June 25, 1991. This work was supported in part by grants from the National Cancer Institute, CA29653 and CA39468.

S. A. Haider and T. C. Cetas are with the Radiation Oncology Department, College of Medicine, and the Department of Electrical and Computer Engineering, University of Arizona, Tucson, AZ 85724.

J. R. Wait is with the Department of Electrical and Computer Engineering, University of Arizona, Tucson, AZ 85724.

J.-S. Chen is with the Radiation Oncology Department, College of Medicine, University of Arizona, Tucson, AZ 85724.

IEEE Log Number 9102814.

implant diameter is much smaller than both the free space wavelength and the implant length, we may assume that H_z varies only insignificantly in the ϕ and z directions. Thus (1) is reduced to a modified Bessel's equation of order zero with the solution:

$$H_z(\rho) = AI_0(\gamma\rho) + BK_0(\gamma\rho), \qquad \text{for } 0 \leqslant \rho \leqslant a \quad (3)$$

where I_0 and K_0 are modified Bessel's functions of first and second kind of order zero. The arbitrary constants, A and B, are to be determined from boundary conditions which require that the field be finite at $\rho = 0$ and H_z being tangential to the implant surface be continuous at $\rho = a$. Therefore, B must be zero to prevent a singularity at $\rho = 0$. The magnetic field has a radially varying axial component H_z given by

$$H_z(\rho) = \frac{H_0}{I_0(\gamma a)} I_0(\gamma\rho), \qquad \text{for } 0 \leqslant \rho \leqslant a \quad (4)$$

where H_0 is the magnetic field at the implant surface. The corresponding electric field as determined from Ampere's law has an azimuthal component, E_ϕ, as follows:

$$E_\phi(\rho) = \frac{-\gamma H_0}{(\sigma + j\omega\epsilon)} \frac{I_0'(\gamma\rho)}{I_0(\gamma a)}, \qquad \text{for } 0 \leqslant \rho \leqslant a \quad (5)$$

where I_0' is the derivative of I_0 with respect to its argument.

Integrating the resulting radial component of the Poynting vector over the implant cylindrical surface of unit length, the power absorption per unit length of the implant for an axially parallel magnetic field is given by

$$P_{\|} = -(2\pi a) H_0(1/2) \operatorname{Re}\{E_\phi(a)\}$$
$$= \pi a |H_0|^2 \operatorname{Re}\left\{ \frac{\gamma I_1(\gamma a)}{(\sigma + j\omega\epsilon) I_0(\gamma a)} \right\} W/m \quad (6)$$

where the identity $I_1(z) = I_0'(z)$ has been used and Re denotes the real part of the quantity within the parentheses. Equation (6) can be rewritten equivalently as follows:

$$P_{\|} = \pi a |H_0|^2 \operatorname{Re}(Z_s) W/m \quad (7)$$

where

$$Z_s = \frac{\gamma I_1(\gamma a)}{(\sigma + j\omega\epsilon) I_0(\gamma a)} \quad (8)$$

is the surface impedance [4] at $\rho = a$. When the implant is highly conducting ($2.0\times10^6 \sim 3.0\times10^6$ S/m) or the frequency (range mentioned above) is low enough such that $\epsilon\omega/\sigma \ll 1$, (2) can be approximated by

$$\gamma a \simeq (j\omega\mu\sigma)^{1/2} a = x e^{j\pi/4}. \quad (9)$$

In (9) the quantity

$$x = (\omega\mu\sigma)^{1/2} a \quad (10)$$

is defined as the induction number of the implant. Then the Bessel functions of argument $x\exp(j\pi/4)$ can be expressed conveniently in terms of Kelvin's ber and bei functions [5] so that

$$P_{\|} = \pi(x/\sigma)|H_0|^2 f(x) W/m \quad (11)$$

where

$$f(x) = \frac{\operatorname{ber}(x)\operatorname{ber}'(x) + \operatorname{bei}(x)\operatorname{bei}'(x)}{\operatorname{ber}^2(x) + \operatorname{bei}^2(x)}. \quad (12)$$

The power absorption per unit volume of cylindrical implant from axially parallel field is found by normalizing (10) with respect to πa^2:

$$\tilde{P}_{\|} = (\omega\mu/x)|H_0|^2 f(x) W/m^3. \quad (13)$$

Plots of $P_{\|}$ as a function of x are shown in Fig. 1 for different values of conductivities and a magnetic field strength of 1500 A/m. The power absorption per unit length increases almost linearly with induction number and hence with radius, a, for fixed ω, μ, σ. Alternatively, it increases as the square root of frequency for fixed μ, σ and a. Fig. 2 shows plots of $\tilde{P}_{\|}$ versus x for various relative permeabilities μ_r. This function maximizes at $x = 2.5$ which implies that optimum power absorption per unit volume occurs when the induction number is 2.5. Existence of such an optimal condition was noted earlier by Wait [4] and by Matsui *et al.* [13] although neither suggested a design for an implant that exploits this optimization, as we do in the next section. The induction number is simply an alternative representation of the ratio of the radius of the implant to the skin depth, δ. Thus we may note that

$$x = \sqrt{2}a/\delta,$$

where

$$\delta = (2/\omega\mu\sigma)^{1/2}.$$

In designing an implant for optimum power absorption the induction number should be close to its optimum value 2.5, or alternatively when the ratio of the radius to the skin depth is: $a/\delta = 2.5/\sqrt{2} = 1.77$. For a particular implant material (i.e., for specific values of μ and σ) at each operating frequency there is an optimum radius for maximum power absorption per unit volume. Fig. 3 shows the optimum radius versus frequency for various values of relative permeabilities and a typical value of electrical conductivity ($\sigma = 2.2\times10^6$ S/m).

Ferromagnetic Implant Design Example

In clinical hyperthermia treatments [6], [7] we formerly used solid cylindrical shaped implants of diameters 1 to 1.5 mm. The frequency of the applied magnetic field typically is about 90 kHz but useful frequencies range from 50 kHz to 500 kHz [7]. The power absorption in implants can be increased several fold using appropriate numbers of implants with optimal diameter to fit into the same cross-sectional area as an encapsulated solid implant. As a practical example which we have constructed and used, six cylindrical filaments of diameter 0.45 mm can be accommodated in a cylinder of diameter 1.4 mm as

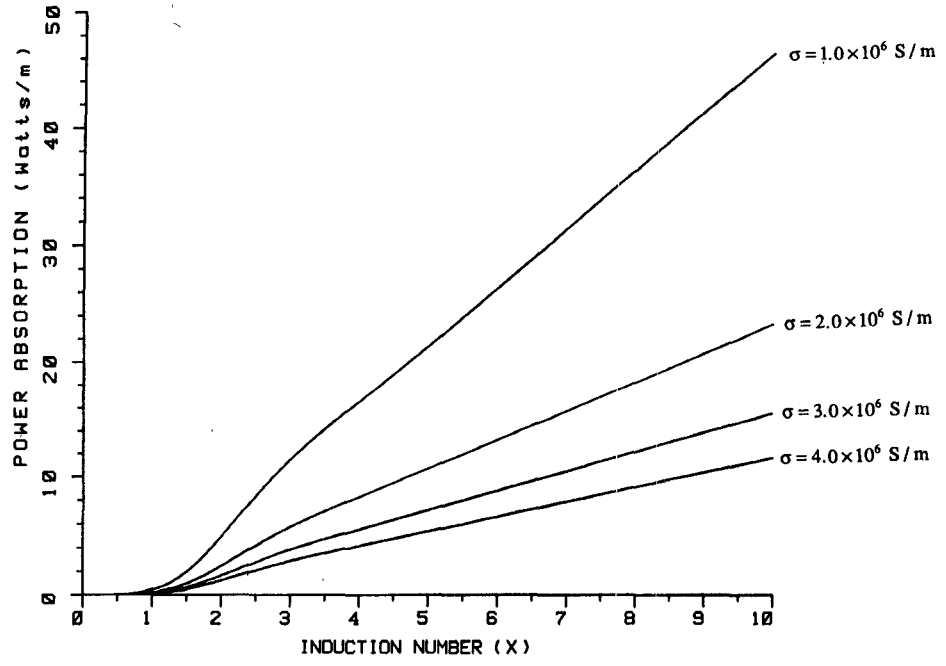

Fig. 1. Absorbed power per unit length of a cylindrical implant in axially parallel magnetic field of strength 1500 A/m as a function of induction number x for different values of electrical conductivities.

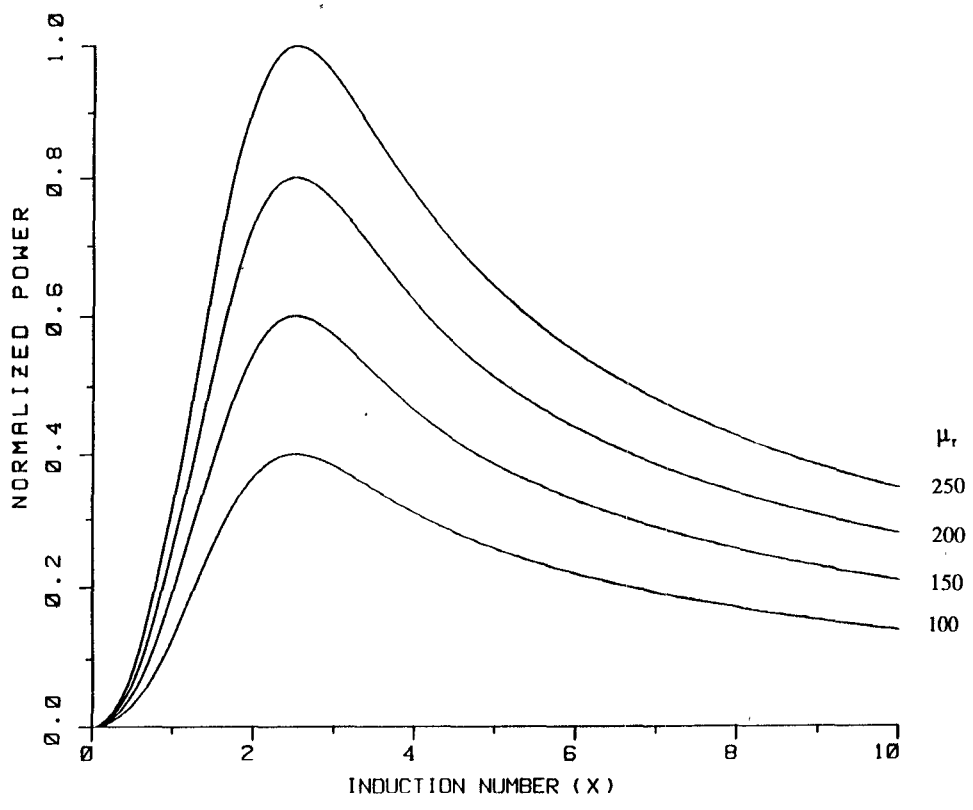

Fig. 2. Power absorption per unit volume of cylindrical implant in axially parallel magnetic field as a function of induction number x for different values of relative permeabilities. Here power absorption per unit volume is normalized with respect to the maximum power absorption of the implant with relative permeability 250.

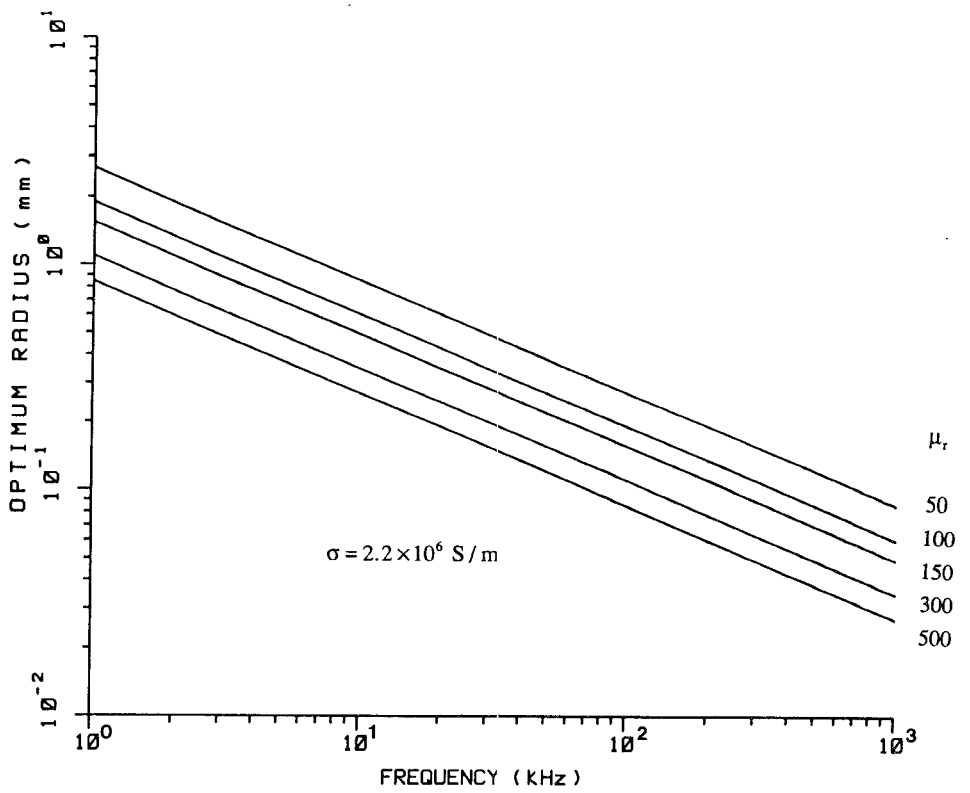

Fig. 3. Optimum radius of a cylindrical implant (in parallel magnetic field) versus frequency for various values of relative permeabilities with electrical conductivity, 2.2×10^6 S/m.

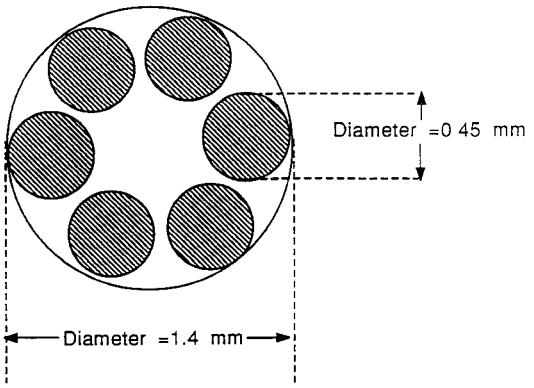

Fig. 4. Stranded or composite implant configuration for optimum power absorption. Cross-section of a 1.4 mm diameter solid implant replaced by six strands of wire with diameter 0.45 mm.

shown in Fig. 4. If electrical conductivity, relative permeability and operating frequency are 2.2×10^6 S/m, 150, and 100 kHz, respectively, then a solid implant of 1.4 mm diameter would absorb approximately 24 W/m from a magnetic field of amplitude 1500 A/m, whereas a stranded wire implant as described above would absorb approximately 40 W/m from the magnetic field of same strength. This is more than a 60% increase in absorbed power. Table I shows a comparison of absorbed power for solid and stranded wire implants of comparable diameter at various frequencies. Note that the diameter of 0.45 mm is somewhat larger than the optimal value of 0.3 to 0.4 mm as suggested by Fig. 3. This was for two reasons. First, it is better to be off on the side of higher induction number x, since the total power absorption is greater (Fig. 1) and the departure from optimal conditions is not as steep (Fig. 2). We do not have reliable values for μ, *a priori*, since the magnetic properties are extremely sensitive to the history of the sample, including its state of internal stress, its microscopic composition, and its local crystallographic properties. The second reason will become clear in a later section.

Calorimetric measurements of power absorption in both types of implant configurations confirm the calculated increase in absorbed power in an implant of stranded filaments. Calorimetric measurement data shown in the Tables II-A and II-B were carried out at different times for different implant materials subjected to different applied powers in the same coil. Table II-B represents the most recent data. For comparison convenience, the data are normalized for 1 kW of applied coil power which corresponds to 726 A/m H-field strength. This was possible due to the linear relationship between applied power and the square of the H-field of the coil. Tables II-A and II-B are self-explanatory and the normalized units W/m-kW and W/cm^3-kW represent power absorption per unit length and per unit volume of the implants, respectively for 1 kW of applied coil power.

Power absorption data for these materials were obtained using an adiabatic calorimeter (shown in Fig. 5) which consists of a cylindrical quartz glass tube with a narrow neck for thermocouple insertion, contains 15 cm^3 of water and will handle implants up to 5 cm long. This

TABLE I
CALCULATED POWER ABSORPTION FOR SOLID AND STRANDED IMPLANTS

Freq. f kHz	Rel. Perm. μ_r	Elect. Cond. σ(S/m)	Induction Number (x) Solid 1.4 mm (dia.)	Induction Number (x) Solid 0.45 mm (dia.)	Power Absorption (W/m) Solid 1.4 mm (dia.)	Power Absorption (W/m) Solid 0.45 mm (dia.)	Power Absorption (W/m) Stranded 6 Filaments of 0.45 mm (dia.)
100	150	2.2×10^6	11.30	3.60	24.04	6.70	40.22
90	150	2.2×10^6	10.72	3.44	22.72	6.28	37.70
80	150	2.2×10^6	10.11	3.24	21.33	5.82	34.94
70	150	2.2×10^6	9.45	3.03	19.84	5.30	31.82

TABLE II-A
CALORIMETRIC MEASUREMENT OF IMPLANT POWER ABSORPTION

Implant Material Designation*	Implant Configuration (Solid or Stranded)	Power Absorption Per Unit Length (W/m-kW) Solid or Stranded	Power Absorption Per Unit Length (W/m-kW) Per Filament in Stranded	Volume W/cm^3-kW
NiZ4	Solid Implant dia. = 1.0 mm	3.38		4.3
AME206	Solid Implant dia. = 1.0 mm	3.05		3.88
AME206	Stranded Implant 6 filaments of dia. = 0.46 mm	6.53	1.09	6.55
AME206	Stranded Implant 4 Filaments of dia. = 0.46 mm	5.38	1.35	8.09

Test Conditions: Applied Power: 4 kW
H-field Strength: 1452 A/m
Frequency: 82.7 kHz

*These materials are all nominally 96% Ni and 4% Si, although actual composition may vary between batches. Furthermore, magnetic properties are dependent upon the homogeneity of composition, the amount of residual stress in the sample and on the crystalographic structure. Hence batch designations are necessary.

TABLE II-B
CALORIMETRIC MEASUREMENT OF IMPLANT POWER ABSORPTION

Implant Material Designation	Implant Configuration (Solid or Stranded)	Power Absorption per Unit Length (W/m-kW) Solid or Stranded	Power Absorption per Unit Length (W/m-kW) Per Filament in Stranded	Volume W/cm^3-kW
Niz4	Solid Implant dia = 0.98 mm	3.48		4.61
AGA160	Stranded Implant 6 Filaments dia = 0.39 mm	8.09	1.35	11.20
AGA160	Stranded Implant 4 Filaments dia = 0.39 mm	5.79	1.45	12.12
AGA160	Stranded Implant 3 Filaments dia = 0.39	4.60	1.53	12.84
AGA160	Stranded Implant 2 Filaments dia = 0.39 mm	3.12	1.56	13.06

Test Conditions: Applied Power: 1.5 kW
H-field Strength: 889 A/m
Frequency: 82.7 kHz

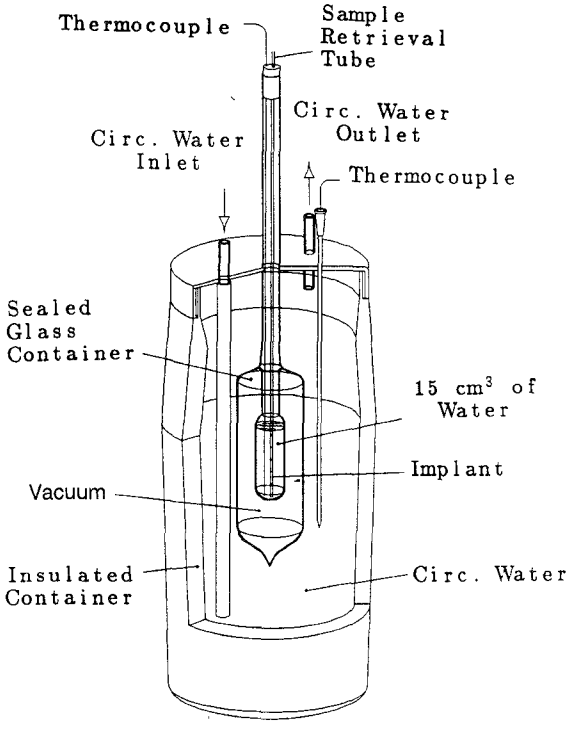

Fig. 5. Diagram of the calorimeter.

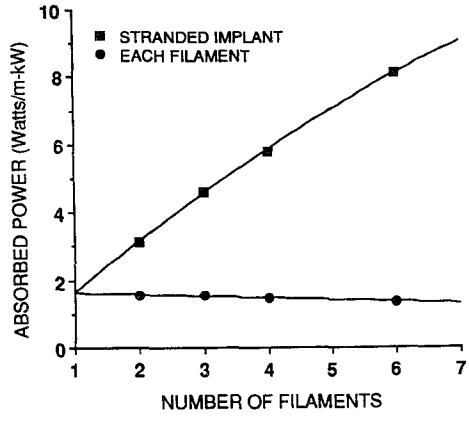

Fig. 6. Calorimetrically measured power absorption in stranded wire implants (material type designation: AGA160, data from Table II-B) versus number of constituent filaments in it. Power absorbed by each filament is determined by dividing measured power absorption of the stranded implant by its constituent filament numbers. Solid lines are polynomial fit to the data.

tube is isolated from the surrounding larger glass tube by a vacuum. The complete glassware assembly was placed inside a plastic insulated container. Temperature regulated water circulated in the plastic container. The water temperature closely tracked the rising temperature in the glass tube calorimeter in order to minimize radiation heat losses from the inner calorimeter chamber. The implant was immersed in 15 cm^3 water inside the calorimeter and was heated by an impressed radio frequency magnetic pulse of a few minutes duration. A number of multisensor thermocouples recorded water temperatures via an automated thermometry data acquisition system (DAS). Right after power was switched off, the calorimeter was shaken to equilibrate the water temperature within the calorimeter. The final temperatures were all within a spread of 0.1°C, the resolution of DAS. The total power absorbed was calculated from $P = \Sigma m_i c_i \Delta T / \Delta t$ where m_i's are masses (water, glass bulb etc.) and c_i's are their corresponding specific heats; ΔT and Δt are temperature rise and duration of heating, respectively. Power absorption data were taken at temperatures well below ($\sim$ 20°C) the Curie points of the ferromagnetic materials to avoid problems from significant temperature dependence of absorbed power.

Tables II-A and II-B experimentally confirm the computations showing heating efficiency of stranded wires which are of a diameter approaching the optimum indicated by Figs. 1–3, over a larger solid implant. As an example (Table II-A): AME206 4-filament (diameter-0.46 mm) stranded implant has 15% less material volume than its solid (diameter = 1 mm) counterpart but absorbs 76% more heat under the same conditions.

The theoretical model describes a single, isolated cylindrical filament, but our application is to use them in bundles in close proximity. The net power absorbed for such a stranded implant could be reduced from the theoretical ideal due to mutual couplings among the filaments. To investigate this thoroughly, stranded implants composed of two, three, four and six optimal diameter filaments were subjected to calorimetric tests. The results are tabulated in Table II-B and presented graphically in Fig. 6 where the power absorption by the stranded implants (upper curve) and power absorption per filament in those implants (lower curve) are plotted as a function of number of composing filaments. Indeed mutual interactions reduce the absorbed power per filament, but only by about 15% between the cases of two-filament implant (minimal interaction) and the six-filament implant which is the highest number tested.

Additionally, we should consider the nature of physical structures required for handling the implants. First, the practical materials must be sufficiently flexible to be able to slip into hollow, plastic tubes which are placed during surgery and which may not be perfectly straight. Second, the "active length" of the ferromagnetic material must correspond to the dimensions of the tumor and should not produce excessive heating of surrounding normal tissues including the normal tissues between the tumor and the skin surface through which the implant enters. In the solid seed configuration, these two constraints were met by stringing together short, 1 cm long, seeds inside heat shrink tubing. The stranded wire implant configuration is intrinsically flexible and also permits use of the central core for other purposes, such as providing a pull-thread (plastic string to pull the implant out of the "after loading" catheter that had been previously placed in the tumor), a thermometer for monitoring implant temperatures, or for containing a radioactive source such as Ir-192 wire. The outer constraining diameter of the ferromagnetic implant thus becomes the inner diameter of the

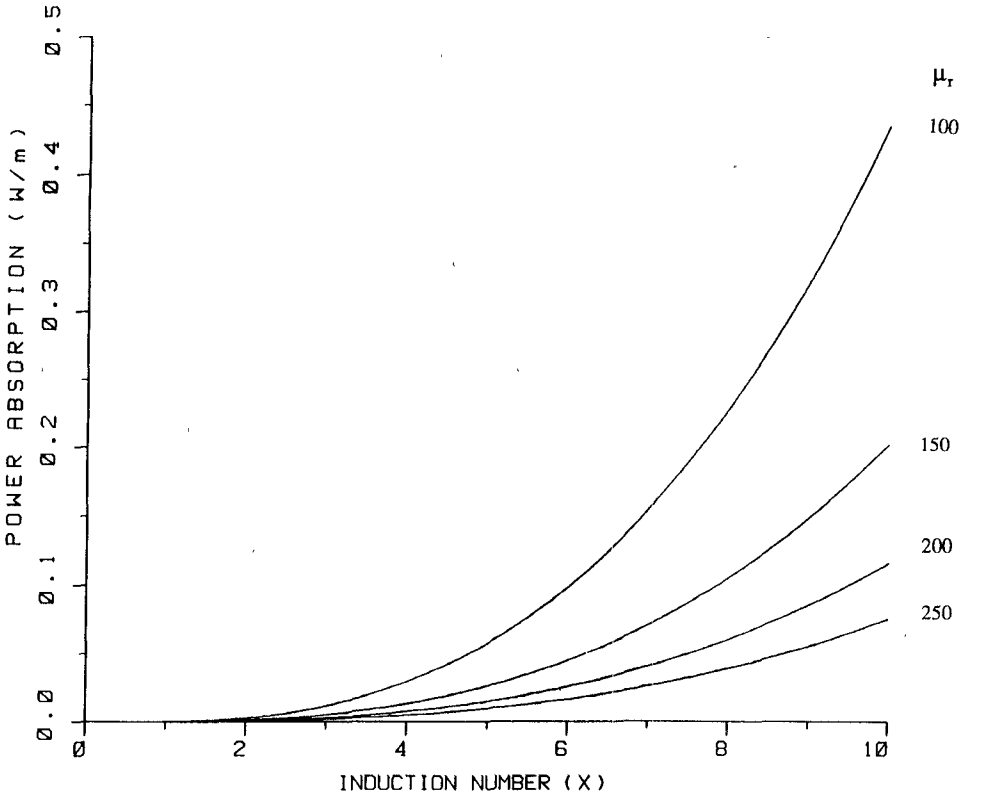

Fig. 7. Absorbed power per unit length of a cylindrical implant in perpendicular magnetic field of strength 1500 A/m as a function of induction number x for various values of permeabilities and electrical conductivity of 1.0×10^6 S/m.

catheter which yields more efficient filling of the available space. A practical six-filament configuration can now be placed into a tube that permitted only a 1 mm diameter seed plus its jacket. The net gain in efficiency is 100%. Finally, it should be noted that the central core would be of little value magnetically because of the shielding effect of the outer filaments.

Power Absorption from Magnetic Field Perpendicular to Axis

In order to investigate the dependence of power absorption of a cylindrical implant on the orientation of the field with respect to its axis in a simple manner, it is necessary to express the power absorption per unit length in a perpendicular magnetic field:

$$P_{\perp} = 8\pi(x/\sigma V)H_0^2\{\mathrm{ber}(x)\,\mathrm{ber}'(x) + \mathrm{bei}(x)\,\mathrm{bei}'(x)\}\ W/m \quad (14)$$

where,

$$V = [\eta\,\mathrm{ber}(x) + \chi\,\mathrm{ber}_2(x)]^2 + [\eta\,\mathrm{bei}(x) + \chi\,\mathrm{bei}_2(x)]^2,$$

$$\eta = \mu_r + 1, \qquad \chi = \mu_r - 1 \quad \text{and}$$

$$\mu_r = \text{relative permeability.}$$

The expression (14) is quoted by Atkinson *et al.* [8]. The derivation is provided in the Appendix [9]. The ratio of $P_{\perp}$ to $P_{\parallel}$ is found using (14) and (11) to be as follows:

$$\frac{P_{\perp}}{P_{\parallel}} = 8\{\mathrm{ber}^2(x) + \mathrm{bei}^2(x)\}^2/V. \quad (15)$$

The plots of (14) and (15) are shown in Figs. 7 and 8, respectively. For high μ material, it is noted that power absorption in a perpendicular magnetic field is very small compared to parallel magnetic field.

Power Absorption in Implants Oriented at an Arbitrary Angle with Applied Field

Practical implementation of aligning implants exactly parallel to the direction of magnetic field polarization is difficult. It is therefore necessary to investigate the effect of orientation on power absorption. If an implant is at an arbitrary angle $^{\pm}\theta$ with the field direction then $H_0\cos\theta$ and $H_0\sin(^{\pm}\theta)$ are components of field parallel and perpendicular to the implant axis. Now utilizing (10) and (14) for $P_{\parallel}$ and $P_{\perp}$ and since sine and cosine functions are orthogonal we obtain the following expression for power absorption as a function of orientation angle θ:

$$P(\theta) = P_{\parallel}\cos^2\theta + P_{\perp}\sin^2\theta \quad (16)$$

Normalized plots of $P(\theta)$ versus θ are shown in Fig. 9 along with the experimental data taken from Buechler [10]. It is found that the analytical expression for $P(\theta)$ is in good agreement with these experimental results. If the implanted ferromagnetic seeds in the tumor volume are within 20 degrees of the direction of the applied magnetic

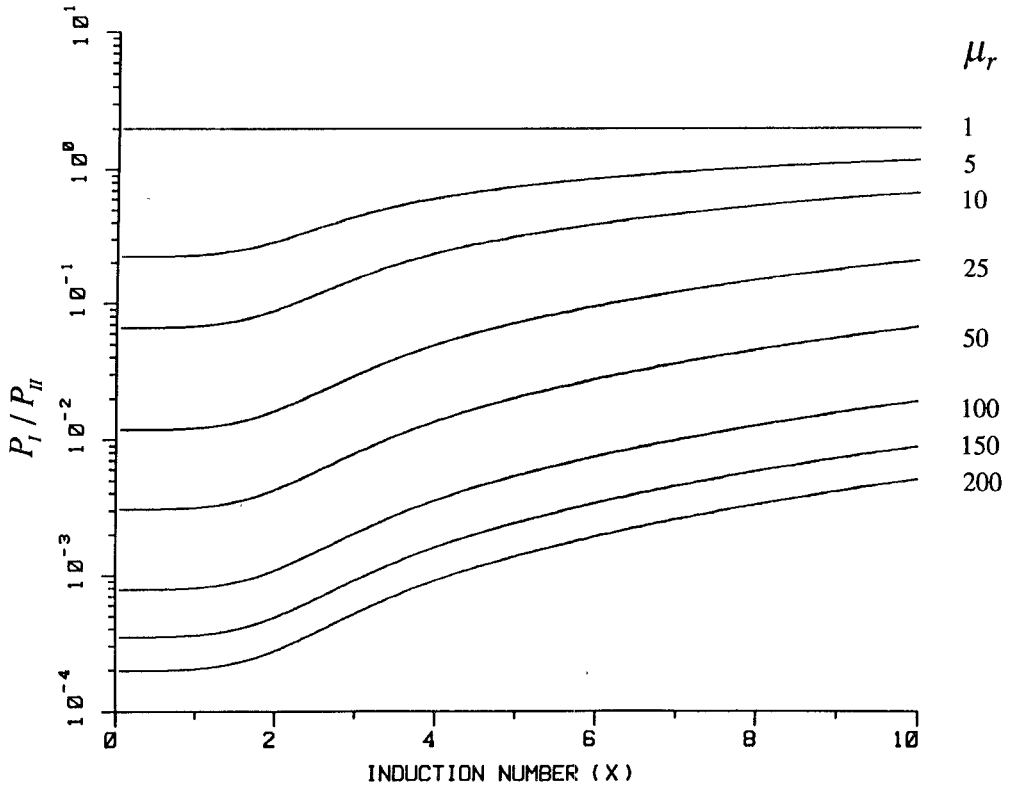

Fig. 8. Ratio of absorbed powers per unit length of a cylindrical implant in perpendicular and parallel magnetic fields as a function of induction number x.

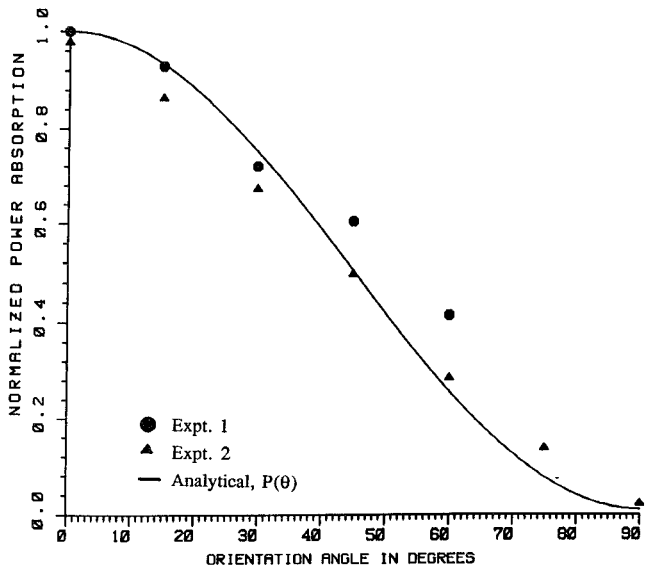

Fig. 9. Absorbed power per unit length of a cylindrical implant as a function of orientation of the implant with respect to polarization of the magnetic field. Here absorbed power is normalized with respect to power absorbed in parallel field. Experimental data taken from Buechler [10].

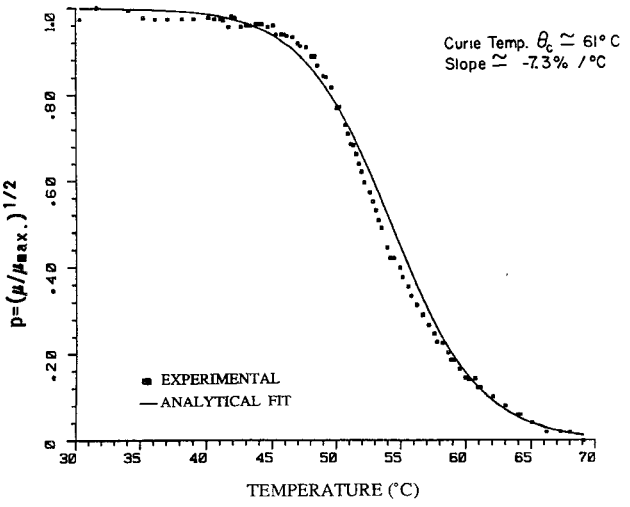

Fig. 10. Figure shows the experimentally measured permeability of Ni-Si ferromagnetic implant as a function of temperature and its fit to closed form empirical expression (17).

field, the power will be about 90% of its maximum value when it is exactly parallel.

Temperature Dependence of Permeability

The particular type of ferromagnetic alloy used for hyperthermia in the clinical trials [6] were produced by Chen *et al.* [1]. These are nickel silicon alloys with Curie transition temperatures in the range of 45° to 80°C. The experimentally measured data on permeability as a function of temperature can be fitted empirically to a closed form analytical function [9] (Fig. 10) characterizing the two basic properties such as Curie point and slope of the curve at linear region:

$$p = \frac{1}{1 + \alpha \exp\left[\beta(T - T_c)\right]} \qquad 0 < p \leqslant 1 \qquad (17)$$

where,

$$p = [\mu(T)/\mu_{\max}]^{1/2},$$

T is temperature, $\alpha = e^2 = 7.389$

a constant and β is related to the slope by

$$\left[\frac{dp}{dT}\right]_{p=1/2} = -\beta/4$$

T_c is the Curie transition temperature defined by the intersection of the tangent of the curve at $p = 1/2$ with the temperature axis. That is T_c is the temperature at which ferromagnetism disappears. It is evident that with increasing temperature, the permeability drops and as a result, the value of the induction number falls from its low temperature value ($T \ll T_c$). In order to maintain high absorption efficiency at temperatures approaching the material Curie point, the designed value of x was chosen above its optimum value 2.5. This is the second reason to which we alluded in an earlier section. When the implant temperature becomes quite close to T_c, then μ drops quickly (Fig. 10), and both the induction number and the power absorption also decrease rapidly. Thus, the transition from high power absorption efficiency to low efficiency becomes steep with respect to temperature.

The conductivity also can be a function of temperatures, but since we are using alloys or Ni (or in some cases Fe) the temperature dependence of the conductivity is small. Measurements in our laboratory [2] show that the intrinsic dc conductivity for these alloys is only insignificantly temperature dependent and the changes in the ac resistance of these metals can be explained by a simple skin depth analysis using $\mu(T)$.

Discussion

The use of inductively heated ferromagnetic seeds for inducing hyperthermia in tumors that can be implanted has been under investigation at a few centers for a number of years. In order to carry out the therapy effectively, it is necessary to understand the conditions that affect the ability of the implants to absorb energy from an applied magnetic field. The results outlined here have influenced the development of this approach in a number of ways.

First, we found that with the original configuration of seeds, the heating of a highly perfused tumor to a therapeutic temperature > 42.5°C was difficult. An increase in implant power absorption was necessary to compensate the power drain by blood flow. The realization of an optimal value for the induction number and the observation that a stranded wire configuration would absorb energy from the field more efficiently led immediately to an alternative implant design. Expected improvements in clinical heating were also observed [12]. Experimental determination of the effects of orientation of the cylindrical implants with respect to the direction of magnetic field followed by its theoretical explanation shows the tolerance of this approach for departures from ideal conditions. That is, while orienting the field with the cylindrical axis of implants is clearly preferred, clinical constraints often make this difficult. From Fig. 9, we note that variation of up to 20° is not critical. Furthermore, if more generator power is available (that is, increased field strength) then orientation mismatches up to 45° can be compensated.

Finally, the empirical representation of the temperature dependence of the permeability can be used in (11), (14), or (16) to yield an analytical expression with these simple, physically relevant parameters (Curie temperature, slope of the transition and power absorption at low temperatures) for power absorption versus temperature for real implants with experimentally determined properties. This expression can be incorporated into the treatment planning/thermal analysis program much more efficiently than could a "look-up" table with an interpolation function.

Conclusion

The efficiency of power absorption depends upon the physical configuration and orientation of cylindrical implants with respect to the magnetic field as well as on the electric and magnetic properties of the implant material. A design is given which results in an efficient implant interms of power absorption, makes efficient use of ferromagnetic material and yields a convenient clinical configuration. A central core in the stranded wire implant is available for a pull-thread, for a thermocouple, or for radioactive seeds for radiation brachytherapy.

Appendix
Power Absorption in Cylindrical Implants from Magnetic Field Perpendicular to Its Axis

The time-harmonic magnetic field which is spatially uniform in absence of the implant, is polarized in the x-direction, therefore can be represented as

$$\vec{H} = \hat{r}H_0 \cos\phi - \hat{\phi}H_0 \sin\phi \tag{18}$$

where H_0 is the amplitude of magnetic field, unit vector $\hat{x}$ has been expressed in terms of cylindrical unit vectors $\hat{r}$ and $\hat{\phi}$ and the time factor $e^{j\omega t}$ has been suppressed for brevity. The incident magnetic field can be derived from the $\hat{z}$-directed magnetic vector potential:

$$\vec{A}^p = \hat{z}A_z^p = \hat{z}H_0 r \sin\phi, \tag{19}$$

by using the definition, $\vec{H} = \nabla \times \vec{A}$.

An infinitely long circular cylinder of radius a with electrical properties (σ, μ, ϵ) is introduced into the otherwise uniform, time harmonic field perpendicular to its axis, which is coincident with $\hat{z}$-axis. No variation along z is assumed (i.e., $\partial/\partial z = 0$). The magnetic vector potential external to the implant ($r > a$) is the superposition of primary and secondary potentials as shown below:

$$\vec{A}^+ = \hat{z}A_z^+ = \hat{z}(A_z^p + A_z^s) \tag{20}$$

where the secondary potential, A_z^s satisfies the Laplace's equation:

$$\nabla^2 A_z^s = 0, \qquad \text{for } r > a \tag{21}$$

with the property that A_z^s is regular at infinity. The potential A_z^- in the interior region of the implant ($0 \leqslant r \leqslant a$), would satisfy the scalar Helmholtz's equation:

$$(\nabla^2 - \gamma^2) A_z^- = 0, \qquad \text{for } 0 \leqslant r \leqslant a \tag{22}$$

with the property that, A_z^- is finite at $r = 0$. In (21) and (22) the Laplacian, ∇^2 has the following form:

$$\nabla^2 \equiv \frac{1}{r}\frac{\partial}{\partial r}\left(r\frac{\partial}{\partial r}\right) + \frac{1}{r^2}\frac{\partial^2}{\partial \phi^2}. \tag{23}$$

In (22) the propagation constant is given by, $\gamma = [j\omega\mu(\sigma + j\omega\epsilon)^{1/2}]$. The superscripts "+" and "−" mean external to and within the implant regions, respectively. The general solutions of (21) and (22) subjected to the conditions stated along with are respectively as follows:

$$A_z^s = \sum_{m=0}^{\infty} r^{-m}\left(p_m e^{jm\phi} + Q_m e^{-jm\phi}\right), \qquad \text{for } r > a \tag{24}$$

$$A_z^- = \sum_{m=0}^{\infty} I_m(\gamma r)\left[U_m e^{jm\phi} + V_m e^{-jm\phi}\right], \qquad \text{for } 0 \leqslant r \leqslant a \tag{25}$$

where $m = 0, 1, 2 \cdots$ and P_m, Q_m, U_m and V_m are arbitrary constants. Invoking the continuity of potential (i.e., $A_z^- = A_z^+$) across the implant surface at $r = a$, we can write after rearranging the terms in the resulting equation as follows:

$$H_0 r \sin\phi = \sum_{m=0}^{\alpha} I_m(\gamma r)\left[U_m e^{jm\phi} + V_m e^{-jm\phi}\right] - \sum_{m=0}^{\alpha} r^{-m}\left[p_m e^{jm\phi} + Q_m e^{-jm\phi}\right] \tag{26}$$

From observation of (26) it is found that the existing mode, $m = 1$ exists with $P_1 = -Q_1$ and $U_1 = -V_1$, therefore (24) and (25) can be written as

$$A_z^s = Q_1 H_0 r^{-1} \sin\phi, \qquad \text{for } r > a \tag{27}$$

$$A_z^- = U_1 H_0 I_1(\gamma r)\sin\phi, \qquad \text{for } 0 \leqslant r \leqslant a \tag{28}$$

where Q_1 and U_1 are the only undetermined coefficients to be determined from the boundary conditions. The vector potentials for regions external and interior to the implant therefore can be written respectively as

$$\vec{A}^+(r,\phi) = \hat{z} H_0\left[r + Q_1 \bar{r}^1\right]\sin\phi, \qquad \text{for } r > a \tag{29}$$

$$\vec{A}^-(r,\phi) = \hat{z} U_1 H_0 I_1(\gamma r)\sin\phi, \qquad \text{for } 0 \leqslant r \leqslant a. \tag{30}$$

The appropriate boundary conditions can be expressed as follows:

1) The tangential component of H field is continuous across the boundary at $r = a$. That is,

$$\left.\frac{\partial A^+(r,\phi)}{\partial r}\right|_{r=a} = \left.\frac{\partial A^-(r,\phi)}{\partial r}\right|_{r=a} \tag{31}$$

2) The normal component of B field is continuous across the boundary at $r = a$. That is

$$\left.\frac{\mu_0}{r}\frac{\partial A^+(r,\phi)}{\partial \phi}\right|_{r=a} = \left.\frac{\mu}{r}\frac{\partial A^-(r,\phi)}{\partial \phi}\right|_{r=a}. \tag{32}$$

Application of the boundary conditions (31) and (32) to (29) and (30) yield the required coefficients Q_1 and U_1. Use of recurrence formulas [5] for modified Bessel's of first kind, Q_1 and U_1 can be put in the following convenient forms:

$$Q_1 = \frac{a^2[(\mu - \mu_0)I_0(\gamma a) + (\mu + \mu_0)I_2(\gamma a)]}{[(\mu + \mu_0)I_0(\gamma a) - (\mu - \mu_0)I_2(\gamma a)]} \tag{33}$$

$$U_1 = \frac{4\mu_0}{\gamma[(\mu + \mu_0)I_0(\gamma a) - (\mu - \mu_0)I_2(\gamma a)]}. \tag{34}$$

The magnetic and the electric fields within the interior of the implant can be determined from the magnetic vector potential as follows:

$$\vec{H} = H_0 U_1\left[\frac{\hat{r}}{r} I_1(\gamma r)\cos\phi - \hat{\phi}\gamma I_1'(\gamma r)\sin\phi\right] \tag{35}$$

$$\vec{E} = -\frac{\hat{z} H_0 U_1 \gamma^2}{(\sigma + j\omega\epsilon)} I_1(\gamma r)\sin\phi. \tag{36}$$

Now the calculation of power absorption per unit length of cylindrical implant of radius a, from an external uniform magnetic field perpendicular to its axis is straight forward. Following the earlier procedure for the case of parallel field it can be shown that

$$P_1 = \frac{1}{2}\pi a |H_0|^2 |U_1|^2 |\gamma|^2 \operatorname{Re}\left\{\frac{\gamma}{\sigma + j\omega\epsilon} I_1(\gamma a) I_1'^*(\gamma a)\right\}. \tag{37}$$

In the limit of quasi-static approximation ($\omega\epsilon/\sigma \ll 1$) we find, $\gamma = (j\omega\mu\sigma)^{1/2}$ and $(\sigma + j\omega\epsilon) \simeq \sigma$. Evaluating $|U_1|^2$ and $\operatorname{Re}[\gamma/\sigma I_1(\gamma\alpha) I_1'^*(\gamma\alpha)]$ in terms of appropriate 'ber' and 'bei' functions [5] we get

$$|U_1|^2 = 16/|\gamma|^2 V \tag{38}$$

where

$$V = [(\mu_r + 1)\operatorname{ber} x + (\mu_r - 1)\operatorname{ber}_2 x]^2 + [(\mu_r + 1)\operatorname{bei} x + (\mu_r - 1)\operatorname{bei}_2 x]^2 \tag{39}$$

$$\operatorname{Re}\left[\frac{\gamma}{\sigma} I_1(\gamma a) I_1'^*(\gamma a)\right] = \frac{x}{\sqrt{a\sigma}}[\operatorname{ber} x \operatorname{ber}' x + \operatorname{bei} x \operatorname{bei}' x]. \tag{40}$$

In (39) and (40) $x = (\omega\mu\sigma)^{1/2} a$ and $\mu_r = \mu/\mu_0$ are induction number and relative permeability of the implant, respectively.

Now substituting the values obtained by (38) and (40) in the expression (37) for power absorption, we get (in SI

units):

$$P_{|} = 8\pi a\left(\frac{\omega\mu}{\sigma}\right)^{1/2} \cdot |H_0|^2(\mathrm{ber}\, x\, \mathrm{ber}' x + \mathrm{bei}\, x\, \mathrm{bei}' x)/V \ \mathrm{W/m}. \quad (41)$$

References

[1] J.-S. Chen, D. R. Poirier, M. A. Damento, L. Demer, F. Biancaniellow, and T. C. Cetas, "Development of Ni-4 wt.pct. Si thermoseed for hyperthermia cancer treatment," *J. Biomaterials Res.*, vol. 22, pp. 303–319, 1988.

[2] R. Sinno, "Quality assurance for the clinical ferromagnetic seeds project," M.S. thesis, Electrical and Computer Engineering, University of Arizona, Tucson, 1989.

[3] J. R. Wait, *Introduction to Antennas and Propagation*. London: Peregrinus Ltd., 1986, Ch. 7, 8.

[4] ____, "Ferromagnetic implants in hyperthermia," *IEEE Trans. Biomed. Eng.*, vol. BME-32, no. 9, pp. 707–708, 1985.

[5] M. B. Abramovitz and I. A. Stegun, *Handbook of Mathematical Functions with Formulas, Graphs and Mathematical Tables*. New York: Dover, 1965, ch. 9, pp. 355–388.

[6] K. S. Au, T. C. Cetas, D. S. Shimm, J.-S. Chen, R. Sinno, S. A. Haider, D. N. Buechler, W. R. Lutz, and J. R. Cassady, "Interstitial ferromagnetic hyperthermia and brachytherapy: preliminary results of a Phase I, clinical trial," *Endocurietherapy / Hyperthermia Oncology*, vol. 5, pp. 127–136, 1989.

[7] P. R. Stauffer, T. C. Cetas, and R. C. Jones, "Magnetic induction heating of ferromagnetic heating of ferromagnetic implants for inducing localized hyperthermia in deep seated tumors," *IEEE Trans. Biomed. Eng.*, vol. BME-31, no. 2, pp. 235–251, 1984.

[8] W. J. Atkinson, I. A. Brežovich, and D. P. Chakraborty "Usable frequencies in hyperthermia with thermal seeds," *IEEE Trans. Biomed. Eng.*, vol. BME-31, no. 1, pp. 70–75, 1984.

[9] S. A. Haider, "Ferromagnetic implants in hyperthermia: An analytical, numerical and experimental study," M.S. thesis, University of Arizona, Department of Electrical and Computer Engineering, Tucson, 1988.

[10] D. N. Buechler, "Magnetic induction heating of ferromagnetic implants for hyperthermic treatments of cancer," M.S. thesis, University of Arizona, Department of Electrical and Computer Engineering, Tucson, 1986.

[11] P. R. Stauffer, T. C. Cetas, A. M. Fletcher, DeYoung, M. W. Dewhirst, J. R. Oleson, and R. B. Roemer, "Observation on the Use of Ferromagnetic Implants for Inducing Hyperthermia," *IEEE Trans. Biomed. Eng.*, vol. BME-31, no. 1, pp. 76–90, 1984.

[12] B. Stea, T. C. Cetas, J. R. Cassady, A. N. Guthkelch, R. Iacono, B. Lulu, W. Lutz, E. Obbens, K. Rossman, J. Seeger, A. Shetter, and D. S. Shimm, "Interstitial Thermoradiotherapy of Brain Tumors: Preliminary Results of a Phase I Clinical Trial," *Int. J. Radiat. Oncol. Biol. Phys.*, vol. 19, pp. 1463–1471, 1990.

[13] M. Matsui, T. Shimizu and T. Kobayashi, "Research on Hyperthermia Implant Materials from a Point of View of Material Science," in *Proc. 3rd Annual Meeting of the Japanese Society of Hyperthermic Oncology*, Japan, 1986, pp. 63–64.

Shah A. Haider (S'88) received the B.Sc. Eng. (electrical) degree from the Bangladesh University of Engineering & Technology, Dhaka, Bangladesh in 1977, and the M.S. degree in electrical engineering from the University of Arizona, Tucson. At present, he is working toward the Ph.D. degree at the University of Arizona.

He was awarded the First Prize in the Ninth All Pakistan Science Fair in 1970 and received the National Science and Technological Fellowship in 1977–1978 to work at the Bangladesh Council of Scientific and Industrial Research Laboratories, Dhaka. From 1978 to 1985, prior to joining the University of Arizona, Tucson, he worked as an Assistant Engineer in the Bangladesh Power Development Board, an Electrical Engineer in the Ministry of Electricity, Libya, and an Electrical Engineer in the National Petrochemical Company, Marsa Al-Brega, Libya.

He received the Curtis Carl Johnson Memorial Award of Bioelectromagnetics Society (BEMS) for Best Student Paper (Engineering) presented in its Eleventh Annual Meeting in 1989. His current research interests include numerical techniques in electromagnetics and its application to hyperthermia, microwave engineering and integrated circuit technology. He is a member of Eta Kappa Nu.

Thomas C. Cetas (M'85) received the Ph.D. degree in physics from Iowa State University, Ames, in 1970.

From 1970 to 1973 he was with the National Measurement Laboratory, Sydney, Australia, and from 1973 to 1975 he was with the National Bureau of Standards (now National Institute of Standards and Technology) and the Bureau of Radiological Health, FDA, which later became the Center for Devices and Radiological Health. Since 1975 he has been with the Department of Radiation Oncology, College of Medicine, University of Arizona, Tucson, where his research has been on the physical aspects of hyperthermia for cancer therapy. Presently he is Professor and Director of the Division of Physics in the Department of Radiation Oncology. He holds joint appointments in Electrical and Computer Engineering and in Aerospace and Mechanical Engineering.

Dr. Cetas is on the Executive Board of North American Hyperthermia Group and was president of that society in 1989–1990.

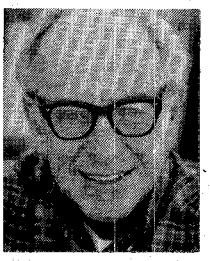

James R. Wait (SM'56–F'62) received the B.A.Sc., M.A.Sc., and Ph.D. degrees from the University of Toronto, Toronto, ON, Canada.

From 1955 to 1980, he was a member of the scientific community in Boulder, CO. His positions included: Senior Scientist in NOAA, Professor Adjoint in E.E. at the University of Colorado, Consultant to the Institute for Telecommunications, and Fellow of the Cooperative Institute for Research in Environmental Sciences. In 1980 he became Professor of Electrical Engineering and of Geosciences at the University of Arizona, Tucson.

Dr. Wait has received numerous awards for his research in electromagnetics and electrical geophysics including the: Balth van der Pol Gold Medal presented by URSI in Helsinki in 1978, IEEE Centennial Medal in 1984, IEEE Geoscience and Remote Sensing Distinguished Achievement Award in 1985, and the IEEE Antennas and Propagation Distinguished Achievement Award in 1990. He is a member of the (U.S.) National Academy of Engineering. In 1988, he was appointed a Regents Professor at the University of Arizona. In 1989, he retired from the university to become a private consultant residing at 2210 East Waverly, Tuscson AZ 85719 (phone: 602-325-1005).

Jong-S. Chen, photograph and biography not available at the time of publication.